Journal of Materials Processing Tech. 302 (2022) 117497

Contents lists available at ScienceDirect

Journal of Materials Processing Tech.

journal homepage: www.elsevier.com/locate/jmatprotec

Hybrid IGA-FEA of fiber reinforced thermoplastic composites for forward design of AI-enabled 4D printing

Yuxuan Yu [a,c], Kuanren Qian [a], Humphrey Yang [b], Lining Yao [b,*], Yongjie Jessica Zhang [a,*]

[a] Computational Bio-Modeling Laboratory, Department of Mechanical Engineering, Carnegie Mellon University, Pittsburgh, USA
[b] Morphing Matter Lab, Human-Computer Interaction Institute, School of Computer Science, Carnegie Mellon University, Pittsburgh, USA
[c] Institute of Artificial Intelligence, Donghua University, Shanghai, China

ARTICLE INFO

Keywords:
4D printing
Design workflow
Isogeometric analysis
Volumetric splines
THB-splines
Hybrid elements
Polycubes
Machine learning
Random forest regressor

ABSTRACT

Fused deposition modeling (FDM)-based 4D printing uses thermoplastics to produce artifacts and requires computational analysis to assist its design processes of complex geometries. Previously, finite element analysis (FEA) has been used to simulate 4D printing deformations, and its accuracy has been computationally and experimentally verified. However, using FEA also leads to several limitations, such as geometric approximation error and the computational time-cost due to the high degrees of freedom. To address these issues, this paper introduces isogeometric analysis (IGA) into the deformation simulations and propounds a composite design by hybridizing FEA and IGA elements to reduce the number of degrees of freedom while maintaining the simulation accuracy. Moreover, since the hybrid IGA-FEA method used for modeling 4D printing structure deformation excludes real-time interactivity, we develop a polycube-based random forest regressor machine learning (ML) model to learn the IGA-FEA-based structural mechanics simulations and provide fast deformation predictions. Given the input actuator block distribution and geometry configurations, our well-trained model can predict the residual stress-induced deformation behaviors of mesh-like thermoplastic composite structures. With an error less than 0.11% and computation speed 20 times faster than hybrid IGA-FEA simulations, our model can create real-time (0.93 s) and truthful (99.89% accuracy) results. The effectiveness of the proposed model is demonstrated with several complex design examples. We believe the presented workflow effectively combines IGA, FEA, ML, and 4D printing to provide a powerful computational tool that enriches the 4D printing design tool box, and brings huge application potentials.

1. Introduction

The concept of self-assembly or the term 4D printing from Tibbits (2014) takes advantage of shape memory materials (SMM). This concept is discussed in Ngo et al. (2018) and can be seen in post-processing actuation to deform the fabricated structure. 4D printing is an emerging technology with great potential. Leung et al. (2019) discusses the traditional fabrication limitation lifted by 4D printing. Deng and Chen (2015) shows the emerging potential of 4D printing through self-folding structures. Davis et al. (2016) demonstrates that 4D printed artifacts using intelligent materials can change shape in specific environment. Deng et al. (2017) shows that the shape changing process can also be accurately modelled. 4D printing was also adopted in bioprinting and food printing. An et al. (2016) presented a perspective on the forms of 4D bioprinting. Champeau et al. (2020) pointed out that hydrogel has the ability to modify its shape upon stimuli and can be used in bioprinting and food printing.

Literature has demonstrated effective methods to predict the deformations of designed 4D printing structures. Previously, Yu et al. (2020) established a physically-based finite element analysis (FEA) model to mechanically simulate the structure deformation. This enables the development of even more effective methods, such as SimuLearn shown in Yang et al. (2020). Yet, using finite element methods as a basis, these methods have limited accuracy due to geometric approximation errors. When handling models with complex geometries, the resulting complex mesh also has high degrees of freedom that burden the computation, leading to long simulation time. As an advanced finite element method, isogeometric analysis (IGA) introduced by Hughes et al. (2005) utilizes spline basis for both geometry and the solution space. It generates accurate simulation results while using fewer degrees

* Corresponding authors.
E-mail addresses: liningy@andrew.cmu.edu (L. Yao), jessicaz@andrew.cmu.edu (Y.J. Zhang).

https://doi.org/10.1016/j.jmatprotec.2022.117497
Received 11 October 2021; Received in revised form 15 December 2021; Accepted 11 January 2022
Available online 13 January 2022

of freedom. In this paper, we propose to use a hybrid IGA-FEA method to greatly reduce the degrees of freedom while having a higher accuracy to simulate more complex 4D-printed geometries. We also develop a polycube-based random forest regressor to increase the accuracy of machine learning (ML) models to make more accurate predictions of the deformation of 4D printing structures.

4D printing uses the same materials as 3D printing. Many types of thermoplastics, such as polyetheretherketone (PEEK) and polyetherketoneketone (PEKK), are widely used in 3D printing to produce even high-end applications. Hu et al. (2019) explore 3D printing techniques with PEEK material, and Singh et al. (2019) investigate 3D printed PEKK material characterizations. Alternatively, PLA is another widely used thermoplastics in 3D printing. It is soft and easily deformable when heated above the glass transition temperature (T_g). In this work, we use Carbon Fiber PLA (CFPLA) to maintain the advantages of flexibility and ease of processing while enhancing mechanical performance. The printed structures are reinforced along the fiber orientations, delivering a high stiffness-to-weight ratio. Since the composite material is made of a PLA matrix, it also remains 3D printable but requires a higher extrusion temperature. Tian et al. (2016) shows that, using FDM techniques, CFPLA can be easily combined with PLA to form two-layer fiber-reinforced composites (FRCs) that have 4D printing characteristics, which are relatively more difficult to achieve with traditional manufacturing approaches. Specifically, the PLA in this FRC structure functions as the active deforming element while the CFPLA provides an enhanced structural rigidity. The deformation behaviors can also be controlled by modulating the thickness, printing speed, extrusion temperature, and aspect ratio of the PLA layers. For an in-depth explanation of these factors, please refer to Yu et al. (2020).

FEA is commonly used to predict the deformation of 4D printed structures. Both material definitions and boundary conditions need to be modeled to enable these simulations. Grijpma and Pennings (1994) have characterized the properties of polymeric materials, including filamentous 3D printing materials like PLA and CFPLA. Soares et al. (2008) used an incompressible, isotropic neo-Hookean hyperelastic material to describe the mechanical response of the stents. The effect of static and dynamic loading on the degradation of PLA stent fibers was investigated in order to further define an incompressible hyperelastic material. Khan and El-Sayed (2013) combined Ogden's compressible hyperelastic model and the generalized Maxwell's model to obtain the linear viscoelastic behavior of biodegradable polymers. In Söntjens et al. (2012), a modified Eyring energy was used to define the viscoplastic behavior of PLA. Eswaran et al. (2011) further explored anisotropy in material modeling. In Bodaghi et al. (2019), a shape memory model was used to define the coefficients of thermal expansion for each print layer. In this paper, both PLA and CFPLA are tested with repeated dynamic mechanical analysis (DMA), and specific models are subsequently proposed to characterize their material properties. We also consider the influence of residual stress and body force on the 4D-printed samples during the deformation process.

However, despite that a physically-based FEA model was established in Yu et al. (2020) to predict the deformation of the designed printing structures, the required high degrees of freedom significantly slow down the computation. It is impossible to obtain prediction results in a real-time and interactive design process. In response, SimuLearn by Yang et al. (2020) used a data-driven approach that combines FEA and ML to create real-time (0.61 s) and truthful (97% accurate) 4D printed material simulators. In that paper, Graph Neural Network (GNN) was used as the ML model to speed up the simulation. Similar to the general GNN pipeline discussed in Zhou et al. (2020), the underlying topology of the grid structure can be abstracted into an undirected weight graph that is compatible with CNN used for velocity field prediction shown in Guo et al. (2016). The machine learning approach is also used for modeling non-linearity of 4D-printed soft pneumatic actuators shown in the review by Zolfagharian et al. (2020). In our paper, we developed an ML algorithm that combines polycube based hexahedral dominant mesh from Yu et al. (2021b), polycube based spline modeling from Yu et al. (2021a), and polycube maps from Tarini et al. (2004) to improve the deformation prediction accuracy for 4D printing structures with the help of random forest regressor. Compared to the GNN used in SimuLearn, the polycube based random forest regressor algorithm yields more accurate predictions because all of the structural information (e.g. the connection and the relative position of vertices) are contained in the polycube structure and the model has less noise. In addition, Simulearn uses multiple intermediate steps that lead to error propagation, while our algorithm does not have such problem. Zolfagharian et al. (2021) combined FEA and ML to predict the bending angle of a 4D-printed soft pneumatic actuator. Linear regression and artificial neural network were compared to determine the suitable machine learning model. Su et al. (2020) used hundreds of experiments to train the model and the prediction error is low. Yu et al. (2020) observed that the high computational cost of data-driven simulation methods is largely caused by the high number of degrees of freedom used in FEA. To effectively lower computational costs without undermining simulation accuracy, we conducted structural mechanics simulations with hybrid IGA-FEA to improve simulation stability while obtaining accurate solutions with comparatively fewer degrees of freedom. Following this workflow, we generated large simulation datasets with physically-based hybrid IGA-FEA models for ML model training.

This paper is laid out as follows. Section 2 provides an overview of our workflow. Section 3 discusses physics behind the deformation behaviors, material properties, and material characterization. These techniques and data are then combined in Section 4 to introduce the IGA modeling and simulations, together with design results derived from the proposed workflow. Section 5 introduces the ML algorithm design and implementation details based on the proposed simulation method as a data set generator. Section 6 gives the comparison between the ML predictions and hybrid IGA-FEA simulation results. Finally, Section 7 draws conclusions and points out potential improvement and future directions.

2. Overview of the workflow

In this paper, we propose a workflow to accurately simulate composite thermoplastic structures' self-morphing behaviors. The proposed workflow consists of three major processes: material characterization, hybrid IGA-FEA modeling, and polycube-based random forest regressor ML learning. As shown in Fig. 1, depending on designated deformation behaviors, the workflow first splits the model into two types of components, PLA and CFPLA. Next, we perform volumetric truncated hierarchical B-splines (THB-splines) construction for the CFPLA components while using FEA elements for the PLA parts. The workflow uses the hexahedral control mesh of CFPLA to construct volumetric THB-splines. Through Bézier extraction, the Hex2Spline software (https://github.com/CMU-CBML/HexGen_Hex2Spline) exports spline information into the BEXT file for LS-DYNA. The workflow then builds hybrid models by combining the volumetric THB-splines (CFPLA) and finite elements (PLA). Hybrid IGA-FEA is performed with known material properties and predefined boundary conditions. For a detailed discussion of isogeometric discretization, we refer readers to IGA implementation of polycube based hexhedral mesh generation and spline modeling in Yu et al. (2021b) and truncated hierarchical spline construction for IGA discussed in Wei et al. (2017). In the end, IGA-FEA-based structural mechanics simulation results are extracted to create a data set for training polycube-based random forest regressor ML models to create real-time and truthful morphing material simulators.

Material characterization. The material properties of PLA and CFPLA are characterized through dynamic mechanical analyses with strip test samples under 80 °C – PLA's glass transition temperature. We refer readers to Yu et al. (2020) for an in-depth discussion of the material properties and the precise material characterization of both PLA and CFPLA.

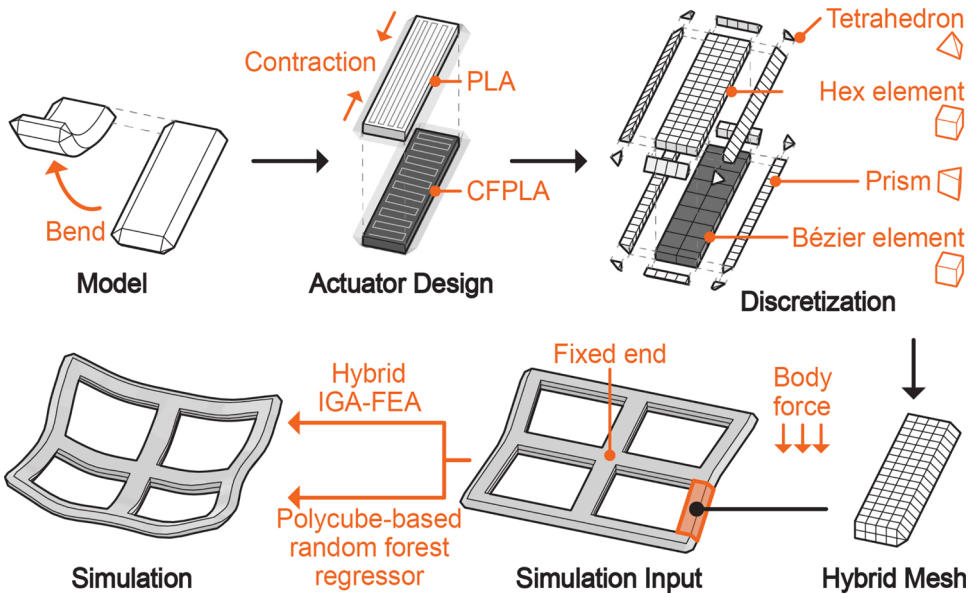

Fig. 1. The workflow of 4D printing design based on IGA simulation: the structure of a block with FEA elements as PLA and IGA elements as CFPLA.

Hybrid IGA-FEA modeling and simulation. The material definition for the hybrid IGA-FEA models is determined based on the material characterization results. The residual stress values are obtained through a shooting method similar to that in Yu et al. (2020). Finally, our IGA implementation includes both the residual stress-releasing and the body force-based creeping processes.

Polycube-based random forest regressor. We develop a polycube-based random forest regressor ML model that learns from the hybrid IGA-FEA structural mechanics simulations and generate fast deformation predictions. Given the input actuator block distributions and geometry configurations, our well-trained model can predict the deformation 4D printed structures with low delay and error.

3. Material characterization

As it was done for the computations reported in Yu et al. (2020), the material properties are collected by performing uniaxial tensile tests on both PLA and CFPLA with the *RSA-G2* equipment under the temperature of 80 °C (see Fig. 2(A)). The PLA material is purchased from *Polymax*, and the CFPLA material is purchased from *Proto-Pasta*, with an average carbon fiber length of less than 150 μm.

Generally, the printing samples are embedded with residual stress along the printing path as the filament is being extruded from the nozzle. Therefore, the samples for material characterization are pre-processed by releasing their residual stress under 80 °C. The Poisson's ratio of the materials can be obtained by measuring the dimensional change of a 3D printed cubic sample before and after the uniaxial compression test. Cubic samples of size 5 mm × 5 mm × 5 mm is printed and subjected to a compressing load perpendicular to the top and bottom surfaces (see Fig. 2(B)). The obtained Poisson's ratio for PLA is 0.419 ± 0.021 and 0.359 ± 0.015 for CFPLA. These results are with an error bound calculated from their 95% confidence interval of measurement. The Poisson's

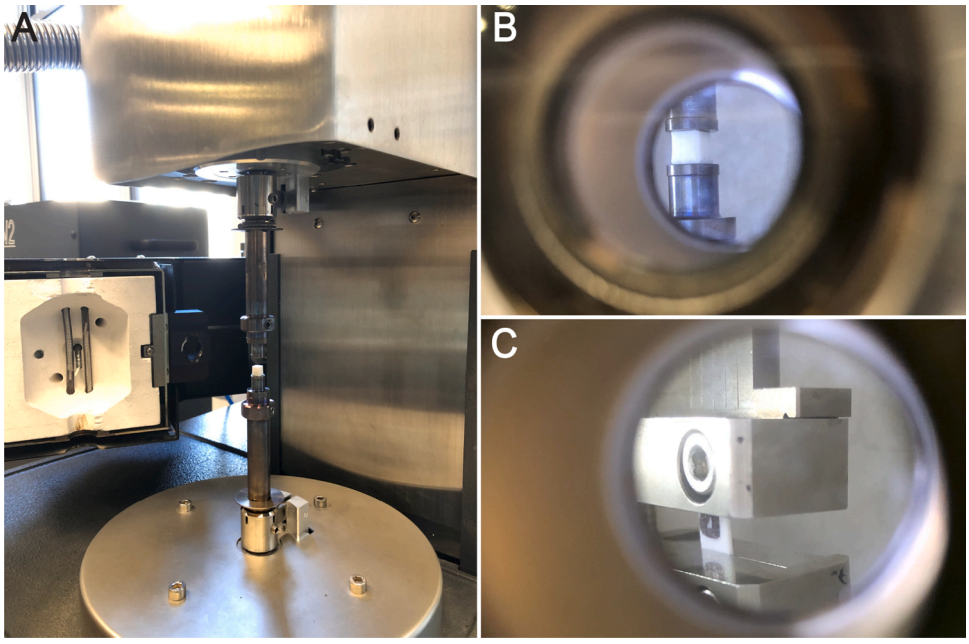

Fig. 2. (A) DMA experiments equipment for material characterization; (B) DMA compression test with a cubic sample; and (C) the tensile test with a strip like sample.

ratio for the computations are set to 0.4066 for PLA and 0.346 for CFPLA. The stress–strain curves are obtained by performing uniaxial tensile tests on a strip sample of size 5 mm × 1 mm × 0.5 mm (see Fig. 2 (C)). We adopt an elastic constitutive model to describe their deformation behaviors. The Young's modulus for PLA is 1.28 MPa and 2.31 MPa for CFPLA. Both are determined by a least-squares fit based on the raw data obtained from the experiments. For the detailed testing procedures of each material property, the readers are referred to Yu et al. (2020).

4. Hybrid modeling for additive manufacturing

The mechanism behind the deformation of 4D printed PLA structures is the residual stress release in response to external stimulation (i.e., temperature above T_g). The application of FEA to predict the deformation of 4D printing structures was reported in Yu et al. (2020). The results have high simulation precision and provide a better understanding of how the designed structures will be affected by the residual stress and body force during the deformation process. Those simulation results can help designers predict the final configuration without having to physically prototype. However, there are two major limitations. The first one is the simulation speed: considering that designers often need to iterate their designs several times before reaching the final product, the time-consuming FEA-based simulators will not be practical in this scenario. Along this line, ML was used in Yang et al. (2020) to speed up 4D printing simulations by three-orders of magnitudes while maintaining high accuracy, but the reported method still requires computing deformations with FEA in advance to generate datasets. The other limitation is the geometry limitation. The 4D printed shoe supporter in Yu et al. (2020) and 4D printed aggregated table in Yang et al. (2020) are simple geometries, which only consist of bending units. However, more complex geometric features are also desirable in certain scenarios. Different types of elements, such as linear tetrahedral and prism elements, are also needed for discretization. Yet, with a more complex mesh, the computational cost also increases accordingly. Our idea is to introduce IGA into the simulation to increase the computational efficiency as IGA can deliver stable and accurate solutions with fewer degrees of freedom. To support even more complex geometries, we use hex-dominant meshes with the hybrid IGA-FEA method.

In this section, we use a bending unit to explain how to construct a multi-patch solid with TH-spline3D for CFPLA (non-degenerated hex domains) and FEA solids for PLA (degenerated and non-degenerated hex domains). Note that Bézier elements cannot be applied with the initial residual stress in LS-DYNA. The bending unit is the fundamental structural unit. It consists of two different blocks – the top actuator block and the bottom constraint block. First, we generate the hex-dominant mesh of this model with hex, tetrahedra, and prism elements as shown in Fig. 3 (A). Then, with the material definition and boundary condition settings, including the fixed region, the body force and the division of actuator and constraint components, we perform the structural mechanics simulation and predict the deformation of this geometry as shown in Fig. 3(B).

We evaluated two design examples completed using the aforementioned process. With our extended workflow, we do not need to use all-hex elements to align geometry features such as fillets, sharp corners with small angles, or prism-like components, which may lead to poor-quality elements. The first simulation example is the top piece of a shoe supporter similar to that shown in Yu et al. (2020). However, the edges of the structure were designed with a fillet to avoid having sharp angles that may harm the wearer.

The structural mechanics simulation results using the hybrid IGA-FEA is shown in Fig. 4(B). The second simulation example is the top piece of the lamp cover from Yu et al. (2020); see the mesh structure and the structural mechanics simulation result using hybrid IGA-FEA in Fig. 5.

We also validated the applicability of the IGA-FEA method in 3D printing. We take a compliant mechanism model (Fig. 6(A)) as an example. The compliant mechanism model transfers forces and motions along the axial directions of the flexural rods, but the rods would bend through elastic deformations when subjected to non-axial loads. The structure is first simplified to end-to-end transmission. We use TH-spline3D for the rod domain (middle section of the model) and use FEA solids for the two ends. Dirichlet boundary conditions are applied to the two ends. The final structural mechanics simulation result is presented in Fig. 6(B). The results validate that we can apply hybrid IGA-FEA and hex-dominant meshes to the compliant mechanism model from 3D printing.

5. Hybrid IGA-FEA-based data-driven simulation

In the previous section, we introduce structural mechanics simulations using a hybrid IGA-FEA method, which can yield stable and accurate solutions with fewer degrees of freedom. However, it is still difficult to predict deformations in real time. To solve this problem, we use our hybrid IGA-FEA implementation to generate datasets for ML model training to further speed up simulations while maintaining an on-par accuracy.

5.1. Polycube-based data generation

To cover the design space of the deforming grid structures, we used a parametric script to generate thousands of similar geometries that have differing geometric parameters. Specifically, the script randomizes the joint locations, and vertices along the edges are linearly interpolated from the randomized joint coordinates. The resulting geometries are topologically equivalent to the initial geometry in Fig. 7(A), which consists of multiple non-degenerated and degenerated cubes. The non-degenerated cubes are modeled with hex elements, whereas the degenerated cubes constructed with prisms and tetrahedrons. The polycube structure has 1108 vertices and 666 elements in total. Next, we build these designs into hybrid IGA-FEA models using the polycube-based and TH-spline3D method, and deformation models were generated and simulated (see Fig. 7(B)). Due to geometric differences, the simulated structures had varying shapes and deformation behaviors.

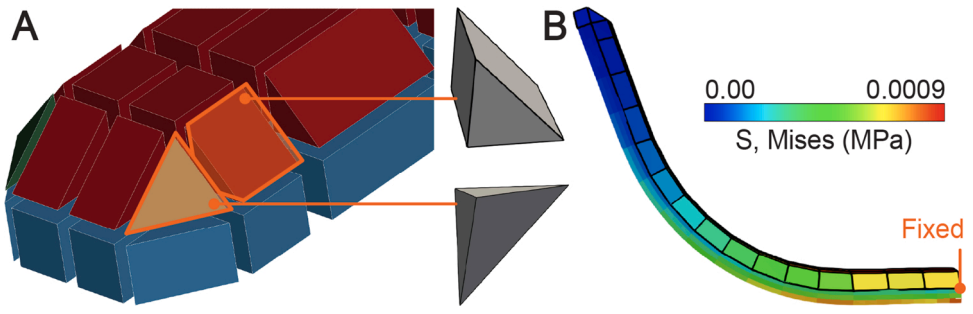

Fig. 3. (A) The hex-dominant mesh of the beam model; and (B) deformation for bending unit structural mechanics computation.

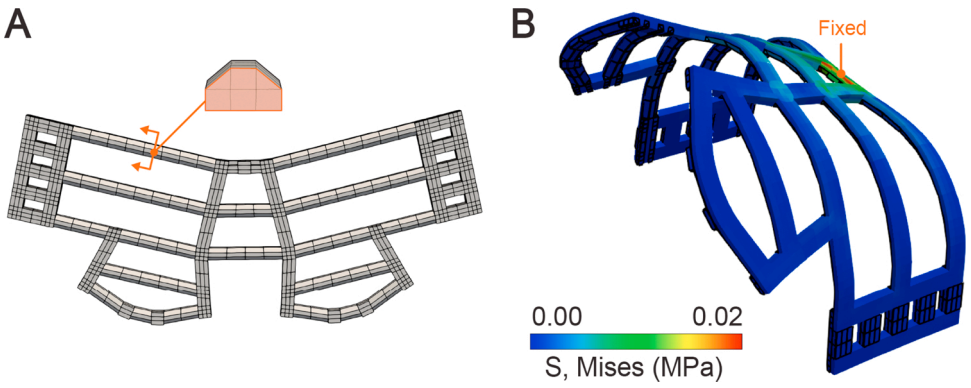

Fig. 4. The structural mechanics simulation of the top piece of the shoe supporter. (A) The structure of the mesh; and (B) structural mechanic simulation result.

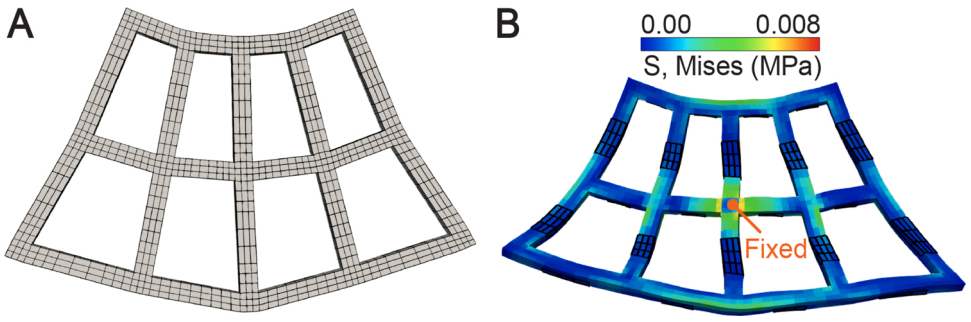

Fig. 5. The structural mechanics simulation of the top piece of the lamp cover. (A) The structure of the mesh; and (B) structural mechanic simulation result.

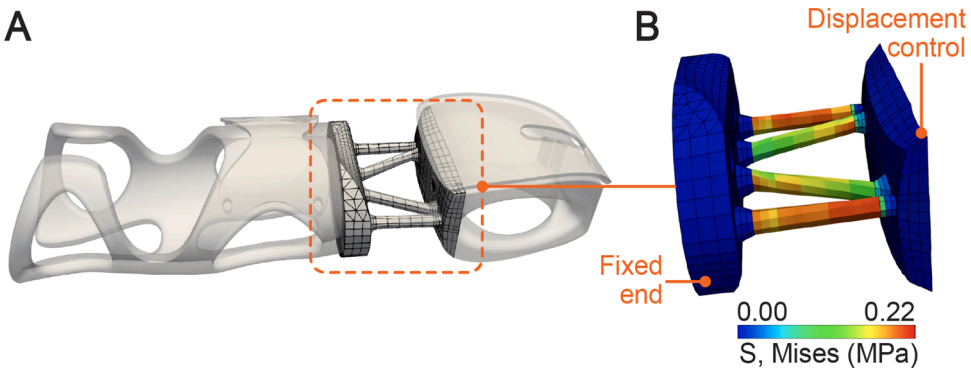

Fig. 6. The structural mechanics simulation of the compliant mechanism model. (A) The structure of the mesh; and (B) structural mechanic simulation result.

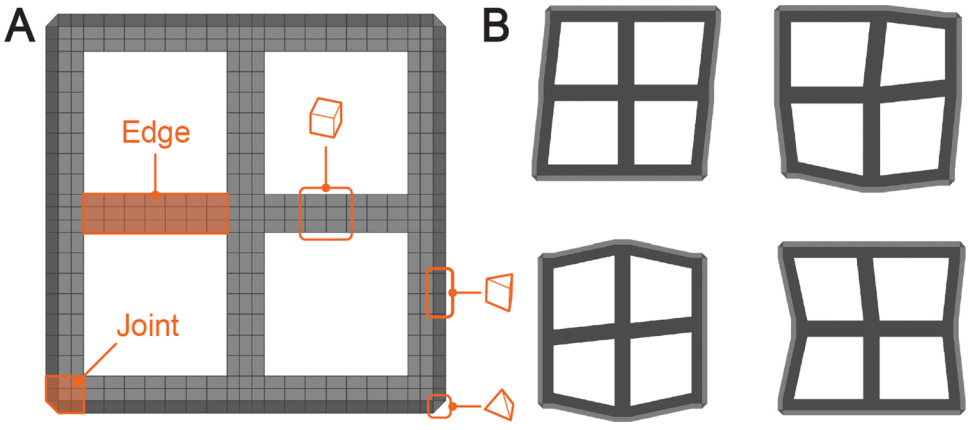

Fig. 7. (A) Polycube structure of all designed printing structure; and (B) samples of the geometry generated by using polycube-based method.

5.2. Polycube-based random forest regressor

Completed hybrid IGA-FEA results are used to extract features for creating ML training data. For each prediction, the deformation result is described by the vertex coordinates. To predict deformation of the structures, we developed a ML algorithm and compared its accuracy and performance with the IGA-FEA model. Fig. 8 illustrates the structure of the developed ML algorithm. We take inspiration from the polycube method and introduce it into ML. Both input and output files are calculated as the displacement with respect to the polycube geometry. For example, the first block of the input feature data is ΔX, which is a $m \times n'$ matrix, where m is the total number of simulations of the training data and n' is the number of coordinates features in x direction (see Fig. 8). In the block, each number is calculated with the equation: $\Delta X = X_g - X_p$, where X_g is the coordinate of one vertex in x direction and X_p is the coordinate of one vertex of polycube geometry in x direction. Take the output as an example, the first block of output data is $\Delta X'$, which is still a $m \times n'$ matrix. In this block, each number is calculated with the equation: $\Delta X' = X_g' - X_p$, where X_g' is the coordinate of one vertex of deformed structure in x direction and X_p is the coordinate of one vertex of polycube geometry in x direction. The multiple random forest regressors are trained to compute the deformation. It consists of 3324 individual random forest regressors. Each regressor is responsible for learning and predicting the displacement at a specific vertex based on a given initial geometry. After learning from all the simulation data, predictions of displacement value from 3324 random forest regressors are combined to create a 2 × 2 mesh grid. The input data for random forest regressor algorithm is a $m \times n$ matrix, where m is the total number of simulations of the training data and n is the number of all features. Each row starts with 3324 initial coordinate information from 1108 vertices or control points, followed by initial residual stress information. The output of each regressor is one displacement value at a specific vertex based on the initial geometry.

5.3. ML results and performance

The performance of the random forest regressor algorithm was evaluated using four metrics: mean square error (MSE), mean absolute error (MAE), coefficient of determination (R^2) based on Pedregosa et al. (2011), and the mean relative error (MRE). For the random forest regressor, 28,125 datasets are split into training and testing data (75/25). Deformations predicted by the 3324 random forest regressor models are compared with their corresponding displacement value in the testing data. The ranges of these four metrics are shown in Table 1. Note that the variance of the design parameters bounds the generalization of the ML model. If the ML model is presented with out-of-range grid design parameters, it is likely to produce less accurate results.

6. ML driven forward design examples

In this section, we demonstrate the broad spectrum of forward design possibilities enabled by the proposed high-accuracy workflow for thermoplastic composites using three forward design examples.

Arm band is the first design implementation of our developed forward design workflow (see Fig. 9(B)). With fast and accurate prediction, our workflow is especially desirable in situations that requires customization, such as personal healthcare equipment. Fig. 9(A) and (B) shows that we can design and combine multiple 2 × 2 grid structures to form a simple arm band structure. The grids had filleted edges to prevent harming the wearer. This combined grid strategy opens up the range of potential applications achievable with the workflow. Using our workflow, this design can be easily changed in real time to customize for different scenarios.

Fig. 9(C) shows the prediction error of the arm band design. To quantitatively measure the accuracy of our model, we compare the displacement differences between hybrid IGA-FEA and ML results. We perform mean relative error (MRE) analysis. The MRE for the arm band design is 0.012%, as shown in Table 2. Compared to hybrid IGA-FEA simulation workflow that takes 19.3 s to complete, our ML driven workflow takes only 0.94 s, approximately 20 times faster.

Lamp cover is the second design of the workflow; see Fig. 10(A) and (B). This design leverages the speed and accuracy of the simulator to iteratively bring the gaps between modules as close as possible, which

Table 1
Comparison between polycube-based random forest regressor and hybrid IGA-FEA.

Metrics	Minimum	Maximum
MSE (mm)	0.0002	0.0354
MAE (mm)	0.00775	0.0873
R^2	0.999916	0.9999995
MRE (%)	0.00899	0.10785

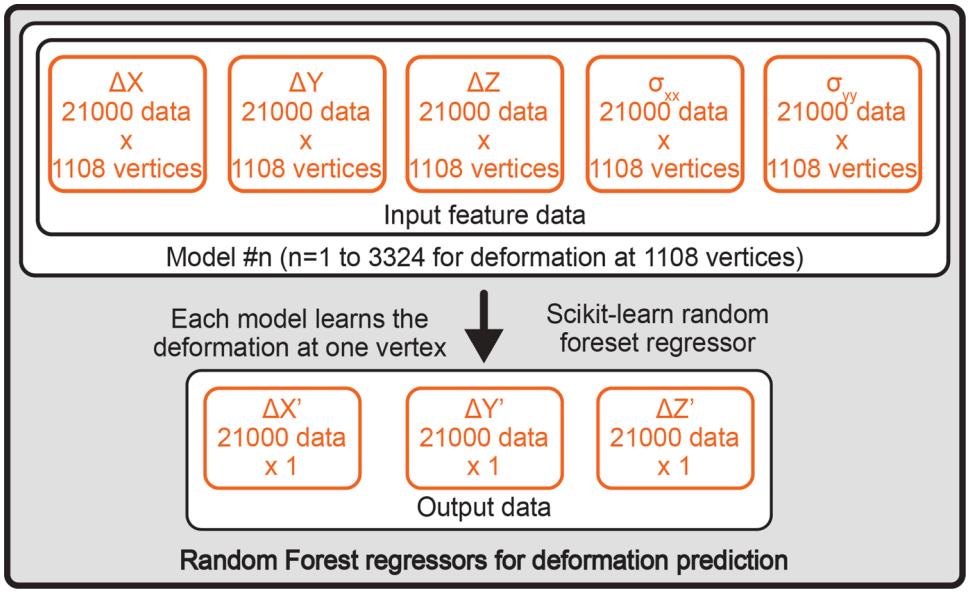

Fig. 8. ML model structure of random forest regressors.

Fig. 9. (A) 2 × 2 grid in arm band design; (B) arm band; and (C) error distribution of arm band design between prediction and ground truth.

Table 2
Statistics of all tested design examples.

Model name	IGA computation time (s)	ML prediction time (s)	MRE (%)
Arm band	19.3	0.94	0.012
Lamp cover	17.0 &19.3	0.94 &0.92	0.037 &0.019
Aggregation sculpture	15.0	0.93	0.07

would have been impossible or impractical without fast and accurate simulator. In this example, multiple 2 × 2 grids are designed to connect and form a complex 3D surface, mimicking a lamp cover.

Fig. 10(C) shows the prediction comparison between hybrid IGA-FEA simulation and ML prediction for lamp cover design. The MRE for lamp cover is measured to be 0.037% and 0.019%. For each 2 × 2 grid, the hybrid IGA-FEA simulation time for top and bottom section of lamp cover are 17 and 19.3 s, while our ML workflow takes only 0.94 and 0.92 s respectively, approximately 19.5 times faster than the hybrid IGA-FEA method.

Aggregation sculpture is the third design using our workflow. We take inspiration from the design in Yang et al. (2020) to further explore the potential complex structures enable by 4D printing and our hybrid workflow. This design starts with a pair of 2 × 2 grids (see Fig. 11(A)). Then, multiple grids are connected to form stack-able rings (see Fig. 11 (C)). By stacking multiple rings with a rotational offset, we can achieve an aggregation structure as shown in Fig. 11(D).

Fig. 11(B) shows the comparison between hybrid IGA-FEA simulation and ML prediction for aggregated sculpture. The MRE for this

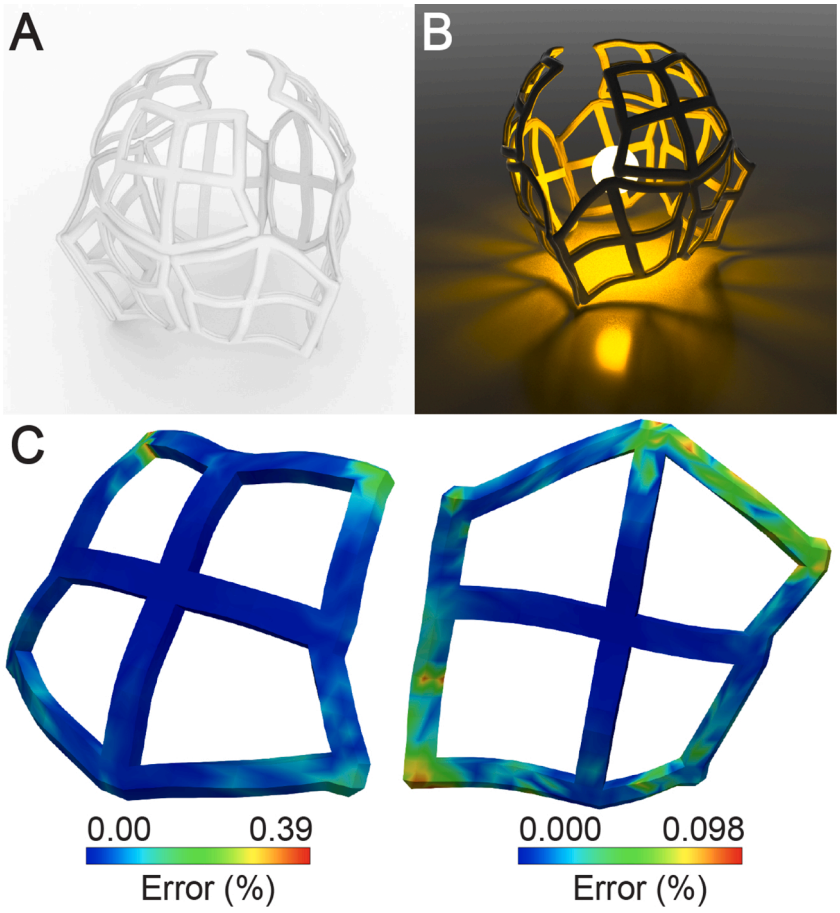

Fig. 10. (A) Lamp cover top view; (B) lamp cover with a light source at the center; and (C) error distribution of lamp cover design between prediction and ground truth.

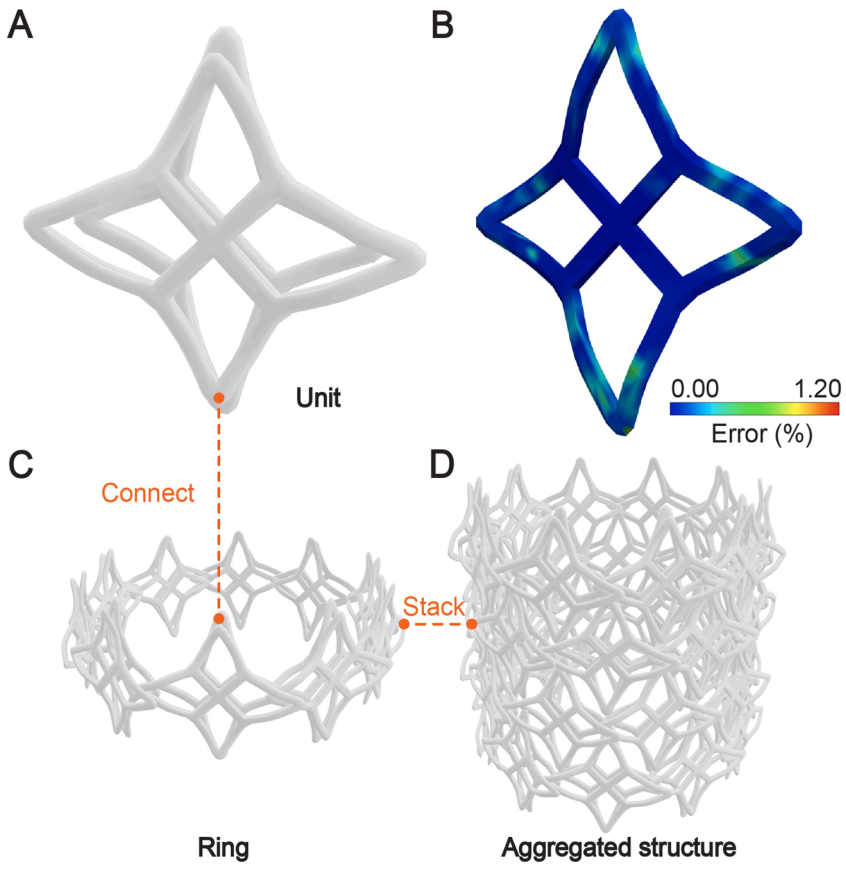

Fig. 11. (A) One aggregation sculpture unit; (B) error distribution of aggregated sculpture design between prediction and ground truth; (C) one ring of aggregation sculpture units; and (D) stacked aggregation sculpture.

design is 0.07%. The hybrid IGA-FEA simulation takes 15 s, while our ML workflow only takes 0.93 s, approximately 16.1 times faster.

7. Conclusion and future work

In this paper, we established a computational workflow that uses hex-dominant meshes, hybrid IGA-FEA, and polycube-based random forest regressor to predict the residual stress-induced morphing deformation behaviors of mesh-like thermoplastic composite structures. By introducing IGA into the deformation simulations and putting forward a composite design by hybridizing FEA and IGA elements, we successfully reduce the degrees of freedom while maintaining the simulation accuracy. This method also significantly speeds up the training dataset generation process for ML. Based on analysis conducted on the developed ML algorithms that use polycube-based method and random forest regressors, our ML algorithm is vastly more efficient and much faster than hybrid IGA-FEA simulation. Our polycube-based ML algorithm also yields good prediction accuracy on deformation. While our workflow is adapted to FDM-based 4D printing, this workflow is also applicable to other 3D printing methods. For example, our workflow can be adapted to particle-based selective laser sintering and selective laser melting where the printing process produces the residual stress. Such residual stress issue was investigated by Mercelis and Kruth (2006) and Meier et al. (2017). In response to external stimulation, the residual stress release can cause the deformation of 4D printed structures. A limitation of our polycube-based random forest regressors algorithm is that the models trained on 2×2 mesh grid is not generalizable to other topologies. For example, it cannot handle 2×3 grid structures. However, it is possible to accommodate these topologies by scaling the polycube models. In that case, retraining is needed if a new topology is introduced. In the future, a data-driven method that extends the geometry model to even more complex mesh structures, instead of only a single 2×2 mesh grid, also worthy additional exploration and can be used to further speed up the simulation. One challenge is reversibility. Application of reversible shape memory to 4D Printing has been investigated by Lee et al. (2019), which has led to significant advances in our understanding of how the heating and cooling as the stimuli to enable reversibility. In this paper, we use PLA and CFPLA as printing material. The irreversible was verified experimentally. However, if we use reversible shape memory, such as hydrogel, we can achieve reversibility by using a combination of stimuli proposed by Lee et al. (2020). A sequential workflow can be developed to achieve accurate simulation results with reversible actuation.

Declaration of Competing Interest

The authors report no declarations of interest.

Acknowledgements

This project was mainly supported by the Carnegie Mellon University Manufacturing Futures Initiative (MFI) made possible by the Richard King Mellon Foundation, the Center for Machine Learning and Health (CMLH) at Carnegie Mellon University, and a Honda grant. We are also especially thankful to Prof. Christopher Bettinger in Departments of Materials Science & Engineering and Biomedical Engineering, who provided the DMA facility. The authors acknowledge the use of the Materials Characterization Facility at Carnegie Mellon University supported by the grant MCF-677785.

References

An, J., Chua, C.K., Mironov, V., 2016. A perspective on 4D bioprinting. Int. J. Bioprint. 2.

Bodaghi, M., Noroozi, R., Zolfagharian, A., Fotouhi, M., Norouzi, S., 2019. 4D printing self-morphing structures. Materials 12, 1353.

Champeau, M., Heinze, D.A., Viana, T.N., de Souza, E.R., Chinellato, A.C., Titotto, S., 2020. 4D printing of hydrogels: a review. Adv. Funct. Mater. 30, 1910606.

Davis, D., Chen, B., Dickey, M.D., Genzer, J., 2016. Self-folding of thick polymer sheets using gradients of heat. J. Mech. Robot. 8, 031014.

Deng, D., Chen, Y., 2015. Origami-based self-folding structure design and fabrication using projection based stereolithography. J. Mech. Des. 137, 021701.

Deng, D., Yang, Y., Chen, Y., Lan, X., Tice, J., 2017. Accurately controlled sequential self-folding structures by polystyrene film. Smart Mater. Struct. 26, 085040.

Eswaran, S.K., Kelley, J.A., Bergstrom, J.S., Giddings, V.L., 2011. Material modeling of polylactide. SIMULIA Customer Conference, Barcelona, Spain May 17–19.

Grijpma, D.W., Pennings, A.J., 1994. (Co) polymers of L-lactide, 2. mechanical properties. Macromol. Chem. Phys. 195, 1649–1663.

Guo, X., Li, W., Iorio, F., 2016. Convolutional neural networks for steady flow approximation. In: Proceedings of the 22nd ACM SIGKDD International Conference on Knowledge Discovery and Data Mining. Association for Computing Machinery, New York, NY, USA, pp. 481–490.

Hu, B., Duan, X., Xing, Z., Xu, Z., Du, C., Zhou, H., Chen, R., Shan, B., 2019. Improved design of fused deposition modeling equipment for 3D printing of high-performance peek parts. Mech. Mater. 137, 103139.

Hughes, T.J.R., Cottrell, J.A., Bazilevs, Y., 2005. Isogeometric analysis: CAD, finite elements, NURBS, exact geometry, and mesh refinement. Comput. Methods Appl. Mech. Eng. 194, 4135–4195.

Khan, K.A., El-Sayed, T., 2013. A phenomenological constitutive model for the nonlinear viscoelastic responses of biodegradable polymers. Acta Mech. 224, 287–305.

Lee, A.Y., An, J., Chua, C.K., Zhang, Y., 2019. Preliminary investigation of the reversible 4D printing of a dual-layer component. Engineering 5, 1159–1170.

Lee, A.Y., Zhou, A., An, J., Chua, C.K., Zhang, Y., 2020. Contactless reversible 4D-printing for 3D-to-3D shape morphing. Virt. Phys. Prototyp. 15, 481–495.

Leung, Y.S., Kwok, T.H., Li, X., Yang, Y., Wang, C.C.L., Chen, Y., 2019. Challenges and status on design and computation for emerging additive manufacturing technologies. J. Comput. Inf. Sci. Eng. 19, 021013.

Meier, C., Penny, R.W., Zou, Y., Gibbs, J.S., Hart, A.J., 2017. Thermophysical phenomena in metal additive manufacturing by selective laser melting: fundamentals, modeling, simulation and experimentation. Annu. Rev. Heat Transfer 20, 241–316.

Mercelis, P., Kruth, J., 2006. Residual stresses in selective laser sintering and selective laser melting. Rapid Prototyp. J. 12, 254–265.

Ngo, T., Kashani, A., Imbalzano, G., Nguyen, K., Hui, D., 2018. Additive manufacturing (3D printing): a review of materials, methods, applications and challenges. Compos. Part B: Eng. 143, 172–196.

Pedregosa, F., Varoquaux, G., Gramfort, A., Michel, V., Thirion, B., Grisel, O., Blondel, M., Prettenhofer, P., Weiss, R., Dubourg, V., 2011. Scikit-learn: machine learning in Python. J. Mach. Learn. Res. 12, 2825–2830.

Singh, R., Singh, G., Singh, J., Kumar, R., 2019. Investigations for tensile, compressive and morphological properties of 3D printed functional prototypes of PLA-PEKK-HAp-CS. J. Thermoplast. Compos. Mater.

Soares, J.S., Moore, J.E., Rajagopal, K.R., 2008. Constitutive framework for biodegradable polymers with applications to biodegradable stents. ASAIO J. 54, 295–301.

Söntjens, S.H.M., Engels, T.A.P., Smit, T.H., Govaert, L.E., 2012. Time-dependent failure of amorphous poly-D,L-lactide: influence of molecular weight. J. Mech. Behav. Biomed. Mater. 13, 69–77.

Su, J.W., Li, D., Xie, Y., Zhou, T., Gao, W., Deng, H., Xin, M., Lin, J., 2020. A machine learning workflow for 4D printing: understand and predict morphing behaviors of printed active structures. Smart Mater. Struct. 30, 015028.

Tarini, M., Hormann, K., Cignoni, P., Montani, C., 2004. Polycube-maps. ACM Trans. Graph. 23, 853–860.

Tian, X., Liu, T., Yang, C., Wang, Q., Li, D., 2016. Interface and performance of 3D printed continuous carbon fiber reinforced PLA composites. Compos. Part A: Appl. Sci. Manuf. 88, 198–205.

Tibbits, S., 2014. 4D printing: multi-material shape change. Architect. Des. 84, 116–121.

Wei, X., Zhang, Y., Hughes, T.J.R., 2017. Truncated hierarchical tricubic C^0 spline construction on unstructured hexahedral meshes for isogeometric analysis applications. Comput. Math. Appl. 74, 2203–2220.

Yang, H., Qian, K., Liu, H., Yu, Y., Gu, J., McGehee, M., Zhang, Y.J., Yao, L., 2020. Simulearn: fast and accurate simulator to support morphing materials design and workflows. Proceedings of the 33rd Annual ACM Symposium on User Interface Software and Technology 71–84.

Yu, Y., Liu, H., Qian, K., Yang, H., McGehee, M., Gu, J., Luo, D., Yao, L., Zhang, Y.J., 2020. Material characterization and precise finite element analysis of fiber reinforced thermoplastic composites for 4D printing. Comput. Aided Des. 122, 102817.

Yu, Y., Liu, J., Zhang, Y.J., 2021a. HexDom: polycube-based hexahedral-dominant mesh generation. SEMA-SIMAI Springer Series: The Edited Volume of Mesh Generation and Adaptation: Cutting-Edge Techniques for the 60th Birthday of Oubay Hassan.

Yu, Y., Wei, X., Li, A., Liu, J., He, J., Zhang, Y.J., 2021b. HexGen and Hex2Spline: polycube-based hexahedral mesh generation and spline modeling for isogeometric analysis applications in LS-DYNA. Springer INdAM Series: Proceedings of INdAM Workshop "Geometric Challenges in Isogeometric Analysis".

Zhou, J., Cui, G., Hu, S., Zhang, Z., Yang, C., Liu, Z., Wang, L., Li, C., Sun, M., 2020. Graph neural networks: a review of methods and applications. AI Open 1, 57–81.

Zolfagharian, A., Durran, L., Gharaie, S., Rolfe, B., Kaynak, A., Bodaghi, M., 2021. 4D printing soft robots guided by machine learning and finite element models. Sens. Actuators A: Phys. 328, 112774.

Zolfagharian, A., Mahmud, M.A.P., Gharaie, S., Bodaghi, M., Kouzani, A.Z., Kaynak, A., 2020. 3D/4D-printed bending-type soft pneumatic actuators: fabrication, modelling, and control. Virt. Phys. Prototyp. 15, 373–402.